Russian Journal of Earth Sciences Online ISSN: 1681-1208

Special Issue: "Kamchatka Earthquake M 8.8 on July 29, 2025"

Gravity Waves Driven by Tsunami after the Kamchatka Earthquake on July 29, 2025

S. A. Riabova[*,1,2] **and S. L. Shalimov**[1]

[1]Schmidt Institute of Physics of the Earth, Russian Academy of Sciences, Moscow, Russian Federation
[2]Sadovsky Institute of Geospheres Dynamics, Russian Academy of Sciences, Moscow, Russian Federation
* **Correspondence to:** Riabova Svetlana, riabovasa@mail.ru

Abstract: The impact of tsunamigenic earthquakes upon the Earth's outer shells provides additional information about the advance approach of tsunamis to infrastructure facilities. This paper examines the measured impact of atmospheric internal gravity waves generated by tsunami propagating after the Kamchatka earthquake on July 29, 2025, upon the ionosphere. The measurements were made at a considerable distance from the earthquake's epicenter (in the Hawaiian Islands). Tidal tsunami monitoring stations recorded the tsunami's arrival, while variations in the ionospheric total electron content were recorded via GPS. Observations have shown that the arrival of tsunami-driven atmospheric waves significantly precedes the arrival of sea waves at the observation point. Attention is drawn to the specific type of variations of the total electron content in the ionosphere and their spectral features, which clearly indicate the early arrival of atmospheric waves at the observation point. Observations have shown that the characteristics of the ionosphere's response to gravity waves generated by sea waves can be used in a tsunami early warning system.

Keywords: Tsunamigenic earthquake, atmospheric gravity wave, total electron content variations, Hawaiian Islands, Kamchatka megathrust earthquake

Citation: Riabova S. A. and Shalimov S. L. (2026), Gravity Waves Driven by Tsunami after the Kamchatka Earthquake on July 29, 2025, *Russian Journal of Earth Sciences*, 26, ES2020, EDN: QHVUVH, https://doi.org/10.2205/2026es001130

1. Introduction

Currently, remote diagnostics of the Earth's outer shells is carried out using global navigation satellite systems (GPS/GLONASS and others) along with a widespread network of ground-based receiving stations, allows the study of rather complex processes of local impact of the lithosphere and ocean on the shells from the rather powerful sources, which are, first of all, earthquakes. These seismic events generate seismic surface waves, which include waves at the boundary of the Earth's surface and the atmosphere (Rayleigh waves), as well as waves at the boundary of the ocean surface and the atmosphere (tsunamis). Both types of surface waves can generate atmospheric waves that propagate vertically. In this paper, we will focus on the impact of tsunamis on the Earth's ionosphere.

Tsunamis are long gravity-driven surface waves. Typically, tsunami periods are several tens of minutes, their wavelengths are several hundred kilometers, and their propagation speed is approximately 200 m/s. Tsunamis can reach several meters in height in the ocean and several tens of meters as they approach the shore. The model proposed in 1967 [*Golitsyn and Klyatskin*, 1967] allows us to establish the possibility of emission of atmospheric waves (both acoustic and internal gravity waves) by seismic waves propagating along the surface of the Earth and ocean. These atmospheric waves serve as a link between propagating seismic waves and the ionosphere, since both acoustic and internal gravity waves have a vertical velocity. Thus, unlike Rayleigh waves, tsunamis cannot emit acoustic waves into the atmosphere, since their horizontal phase velocities are much less than the speed of sound.

Research Article

Received: February 2, 2026
Accepted: May 25, 2026
Published: July 1, 2026

However, tsunamis can emit atmospheric internal waves if the horizontal phase velocity of the atmospheric waves exceeds the velocity of the waves on the ocean surface. This condition only holds for long surface gravity waves, which include tsunamis. Note that in this limit, the horizontal phase and group velocities of the internal atmospheric waves differ by a factor of $\cos(\varphi)$ (here φ is the angle between the wave vector and the horizon). In this case, the group velocity of the waves is greater than or equal to the phase velocity.

Having a vertical velocity component, atmospheric internal gravity waves (IGWs) are capable of reaching the ionosphere (albeit with a delay of about an hour), leading to characteristic variations in plasma density with periods of about 10 min.

Moreover, if the time that takes a tsunami to reach the coast exceeds the time that takes an IGW to reach the ionosphere, then the recorded variations in the density of the ionospheric plasma can be used as an indicator of the imminent approach of a tsunami to the coast.

From the above-mentioned conditions of radiation of atmospheric internal waves driven by a propagating tsunami, it directly follows that the atmospheric wave must precede the tsunami. This conclusion was verified both experimentally (see, for example, [*Azeem et al.*, 2017; *Rozhnoi et al.*, 2012; *Shalimov et al.*, 2017] using measurements that used VLF and GPS radio sounding, and using numerical calculations [*Inchin et al.*, 2022; *Shalimov et al.*, 2017] for one event – the 2011 Tohoku megaearthquake.

Let us note another possible source of atmospheric waves after an earthquake: piston-like displacements of the ocean floor can be transmitted through the hydrosphere into the atmosphere, generating acoustic-gravity waves (AGWs). These waves can propagate through the atmosphere faster than tsunamis and serve as their precursors. It is believed that such atmospheric tsunami precursors, recorded by microbarographs, were observed after tsunamigenic earthquakes: Iturup (1958), Chile (1960), Alaska (1964), etc. [*Soloviev*, 1972]. Unlike IGWs, acoustic waves are capable of reaching the ionospheric layers fairly quickly, where they are transformed into magnetohydrodynamic disturbances. The propagation speed of the latter in the ionosphere can be tens of times greater than that of a tsunami. Therefore, in this case, ionospheric sounding, along with microbarographs, can be used to detect precursor signals, if they can be correctly identified.

In the present paper, measurements from a tsunami tidal monitoring station and GPS measurements of total electron content (TEC) variations are used to examine the impact of a tsunami propagating after an earthquake in Kamchatka and acting upon the ionosphere by means of internal gravity waves driven by the tsunami. Observations have shown that the atmospheric waves generated by the tsunami significantly get ahead the sea waves. Attention is drawn to the specific shape of the ionospheric signals, which clearly indicates the early arrival of the atmospheric wave at the observation point.

2. Initial Data and Methods

To determine the tsunami arrival time on Honolulu Island, we used data from the tsunami forecast model developed by the National Oceanic and Atmospheric Administration (NOAA) for Tsunami Research Center [*NOAA...*, 2025] (Figure 1). A global tsunami propagation forecast was generated by inverting data from three nearby DARTs (Deep-ocean Assessment and Reporting of Tsunamis) using the NOAA forecasting method and the MOST (Method of Splitting Tsunami) model (https://nctr.pmel.noaa.gov/model.html). During tsunami propagation, the model demonstrated good agreement with DART data located at more distant distances, confirming the accuracy of the forecast model [see Composite plot: US Hawaii locations in *NOAA...*, 2025].

Additionally, sea level data from tsunami monitoring stations (https://tidesandcurrents.noaa.gov/tsunami) were used to determine the tsunami arrival time in the Hawaiian Islands. A map of the sensor locations is shown in Figure 2.

In our paper, to analyze the upper ionospheric response we used the GPS satellite data, which allows for the determination of variations in the ionospheric TEC. Navigation

receivers using phase and code ranging measurements allow the TEC to be determined with a high degree of accuracy. When analyzing the ionospheric response, the slant TEC is determined using a combination of phase and code methods, converting the slant TEC to vertical electron content. To isolate the IGW signal, 7th-order Butterworth bandpass filtering was applied to 30-second data [*Butterworth*, 1930]. The Butterworth filter has been identified as a suitable filter for TEC data [*Chandrasekhar et al.*, 2016; *Jayachandran et al.*, 2012; *Wen and Jin*, 2020].

Data from a HNLC station GPS receiver (21.306°N 157.865°W) located on the coast of Honolulu Island served as the input data. The distance to the earthquake epicenter off the coast of the Kamchatka Peninsula is 4963 km.

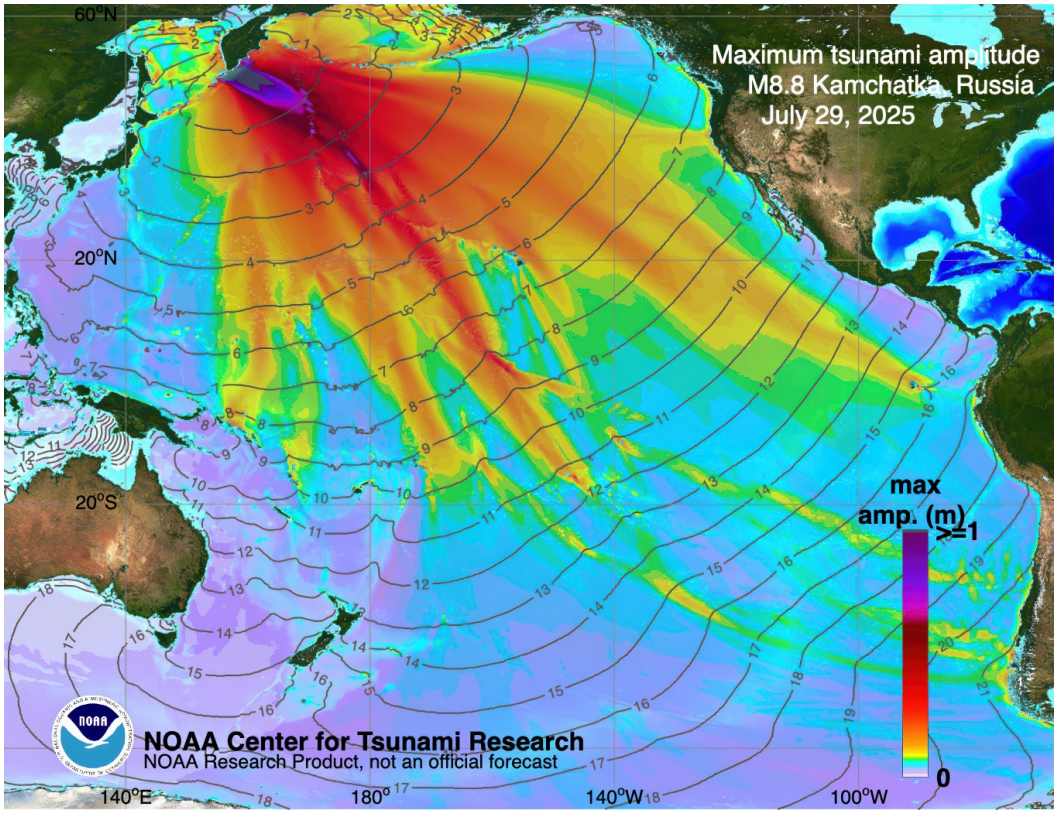

Figure 1. Model of tsunami propagation across the Pacific Basin for the 2025 Kamchatka, produced by the NOAA / PMEL / Center for Tsunami Research [see Figure 2 in *NOAA...*, 2025]. Colors show the maximum tsunami amplitude in the open ocean.

In addition to studying the temporal variations of the TEC, the Earth's magnetic field, their frequency content was also examined. In this study, wavelet analysis was chosen as the spectral analysis method, which has demonstrated its effectiveness in analyzing geomagnetic variations, in particular [*Riabova*, 2022; *Riabova and Shalimov*, 2024a,b,c]. The wavelet transform is a transformation that converts a signal from a time representation to a time-frequency representation and is a convolution of a wavelet function with a signal [*Meyer*, 1993]. The results of the wavelet transform contain combined information about the analyzed signal and the wavelet itself, and also make it possible to isolate low-frequency and high-frequency components of the signal and obtain information about the time at which certain signal components appeared [*Torrence and Compo*, 1998]. In this study, a continuous wavelet transform was used, and the Morlet wavelet was used as the basis wavelet. The presentation of the wavelet transform results is designed in the form of scalograms (local energy spectrum) taking into account the "edge" effects (cone of influence) [*Riabova*, 2018].

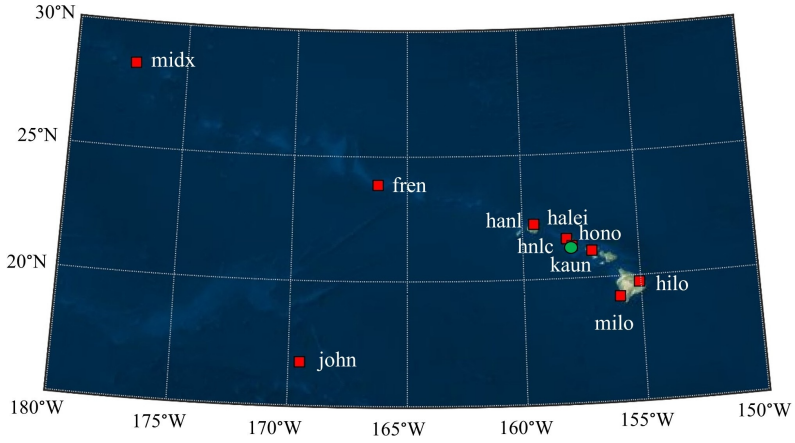

Figure 2. Map of the location of tsunami monitoring stations in the Hawaiian Islands, the location of the GPS receiver (hn1c station) is indicated by a green circle.

3. Description of a Tsunamigenic Earthquake

A powerful earthquake with a magnitude of M_W = 8.8 occurred on July 29, 2025, at 23:24:52 UTC [see Origin in *USGS*, 2025]. The epicenter of the seismic event (52.495°N 160.240°E) was located approximately 125.4 km east-southeast of Petropavlovsk-Kamchatsky [see Regional Information *USGS*, 2025]. The earthquake caused moderate damage in Kamchatskiy Krai and Sakhalinskaya Oblast [see ShakeMap *USGS*, 2025]. In Petropavlovsk-Kamchatsky, the shaking intensity reached VIII on the modified Mercalli scale [see ShakeMap *USGS*, 2025].

The earthquake of July 29, 2025, is the largest in the region since the event of November 4, 1952, which had a magnitude of 9.0 [*USGS*, 2010]. According to the available data, the period between these two strong earthquakes does not seem long enough for the necessary energy reserves to accumulate in the geological environment (practice shows that earthquakes with magnitudes exceeding 7.7 recur every 140–200 years) [*Fedotov*, 1968; *Lobkovsky et al.*, 2021]. In this regard, the opinion was expressed about the uniqueness of the earthquake off the coast of the Kamchatka Peninsula on July 29, 2025 [*Lobkovsky et al.*, 2021]. The earthquake of July 29, 2025, was the strongest event since 2011 and is one of the six largest ever recorded by seismometers, along with the earthquakes of 2010 (Chile) and 1906 (Ecuador–Colombia) [*Wirth et al.*, 2022]. The magnitude 8.8 mainshock was preceded by a foreshock sequence that began in 2024 with a magnitude 7.0 event. Ten days before the mainshock, on July 20, 2025, another foreshock occurred – a magnitude 7.4 earthquake [*Hubbard and Bradley*, 2025].

According to the US Geological Survey, the earthquake occurred on a reverse fault in the Kamchatka subduction zone at a depth of 35 km [see Origin in *USGS*, 2025]. The fault surface was 390 km wide and 140 km long, with vertical displacement of up to 12–12.3 m, with the main part of the rupture located close to offshore suture zones [see Finite fault in *USGS*, 2025]. The earthquake lasted between 180 and 230 seconds (http://geoscope.ipgp.fr/index.php/en/catalog/earthquake-description?seis=us6000qw60). The rupture occurred along the Kuril–Kamchatka subduction zone, one of the most seismically active regions of northeastern Eurasia, where the subduction rate of the Pacific lithospheric plate beneath the North American (Okhotsk) plate reaches 8 cm/year [*Argus et al.*, 2011; *Prytkov et al.*, 2017]. The interaction of the lithospheric plates is accompanied by tectonic deformations that occur both at the plate boundary and in its vicinity [*Koulakov et al.*, 2011]. The subduction zone is a site of the largest tsunamigenic (with a magnitude greater than 8) and deep (more than 600 km) earthquakes [*Bürgmann et al.*, 2005].

The major earthquake of July 29, 2025, triggered not only numerous aftershocks but also a significant tsunami, which was detected by tide gauges and deep-sea instruments throughout the Pacific basin, from Russia to South America [*PTWC*, 2025] (Figure 3). Tsunami warnings and advisories were issued for much of the Pacific region, leading to

coastal evacuations and emergency response measures throughout the region (https://www.reuters.com/business/environment/huge-quake-russia-triggers-tsunami-warnings-around-pacific-2025-07-30/).

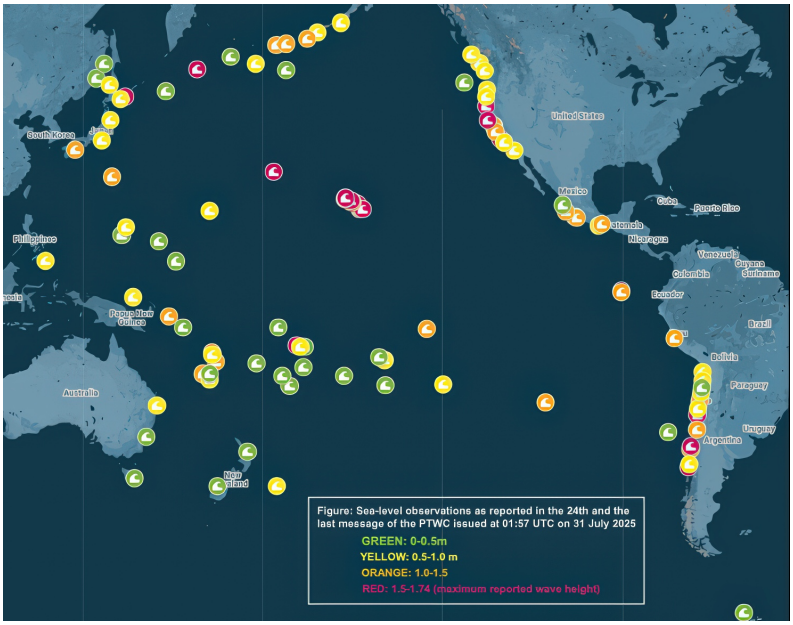

Figure 3. Sea-level observations as reported at 01:57 UT on July 31, 2025 [*PTWC*, 2025] (green: 0–0.5 m, yellow: 0.5–1.0 m, orange: 1.0–1.5 m, red: 1.5–1.74 m as the maximum reported wave height).

The maximum observed amplitudes recorded by the Pacific Tsunami Warning Center (PTWC) were 1.74 m at Kahului (Maui, Hawaii) southeast of the epicenter, 1.13 m at Crescent City (California, USA) east-southeast, 1.04 m at Baltra (Galapagos Islands, Ecuador), and 1.12 m at Coliumo (Chile), both southeast (https://www.ioc.unesco.org/en/global-tsunami-response-m88-kamchatka-earthquake, https://www3.nhk.or.jp/nhkworld/en/news/backstories/4189/) (Figure 3). The tsunami was recorded by eight DART deepwater stations located in the Pacific Ocean [*PTWC*, 2025]. The largest recorded amplitude was 0.85 m off the coast of the Kamchatka Peninsula, closest to the epicenter (DART 21416) [see Figure 3 in *NOAA*..., 2025]. This is the second-largest amplitude ever recorded by DART. The absolute largest amplitude recorded by DART was during the tsunami in Japan on March 11, 2011 (approximately 1.9 m) [*Heidarzadeh and Satake*, 2013]. The DART recording was used to update the tsunami forecast [*NOAA*..., 2025]. Two other DARTs, 21419 and 21415, recorded maximum amplitudes of 31 cm and 25 cm, respectively, within one hour of the earthquake, amplitudes recorded by other DARTs provided by PTWC ranged from 2 to 28 cm [see Figure 3 in *NOAA*..., 2025].

According to preliminary data, during the Kamchatka tsunami, wave heights reportedly reached 5 m in coastal areas near the rupture site, flooding the Severo-Kurilsk port and fish processing plant (https://en.iz.ru/en/1928654/2025-07-30/port-severo-kurilsk-and-industrial-enterprise-are-flooded-after-earthquake), the waves of 3–4 m were observed in the Yelizovsky District of Kamchatka (https://www.themoscowtimes.com/2025/07/30/huge-earthquake-off-far-east-russia-sparks-pacific-tsunami-warnings-a90020), and a 5-meter wave hit Severo-Kurilsk on the nearby Kuril Islands (https://www.vesti.ru/article/4619123). At the Severo-Kurilsk Seaport, a wave surge of 17 m was recorded [*Kotenko et al.*, 2025a]. In the village of Nikolskoye in the Kamchatka region, the wave height reached 6.1 m [*PTWC*, 2025]. On Shumshu Island (Northern Kuriles), the tsunami flooded an area 650 m inland, with waves up to 6 m high and a maximum splash of 19 m [*Kotenko et al.*, 2025b].

4. Arrival of the Tsunami to the Hawaiian Islands

Since a tsunami was generated after the earthquake off the coast of the Kamchatka Peninsula, it is natural to consider it as a source of atmospheric waves.

To ensure that the ocean surface disturbance front has already formed and serves as a source of atmospheric waves (which propagate into the ionosphere), we will analyze observations at a significant distance from the epicenter. Such conditions arise when a tsunami propagates eastward across the Pacific Ocean, passing the Hawaiian Islands in its path (approximately 2/3 of the distance between the Kamchatka Peninsula and Southern California).

In this study, using data from the Honolulu GPS receiving station (hnlc), we examine the ionospheric response to an earthquake centered off the coast of the Kamchatka Peninsula in a zone far from the epicenter.

According to the tsunami forecast model (Figure 1) developed by the Tsunami Research Center of the US National Oceanic and Atmospheric Administration (NOAA), the tsunami reached the Hawaiian Islands approximately 6 hours after the main shock of the earthquake.

Relative sea level variations based on data from tsunami monitoring stations near the Hawaiian Islands (Figure 2) are shown in Figure 4. As can be seen from Figure 4, the tsunami reached the first station, midx, located in the North Pacific Ocean in the western group of the Hawaiian archipelago, at 3:37 UT. According to midx, located 3,272 km from the earthquake's epicenter off the coast of the Kamchatka Peninsula, the sea level height changed by more than 1 m. The tsunami reached the next station, fren, located on the coast of French Frigate Shoals, the largest atoll in the Northwest Hawaiian Islands, at 4:52 UT. This station is located 4,252 km from the earthquake's epicenter off the coast of the Kamchatka Peninsula. The tsunami reached the island of Kauai (hanl, 4,793 km from the earthquake's epicenter) at 5:35 UT, with a wave height of 90 cm. The tsunami reached Johnston Atoll at 5:33 UT (john, 4,773 km from the earthquake's epicenter). The tsunami's arrival on the island of Oahu was recorded at 5:46 UT (halei, 4,932 km from the earthquake's epicenter) and at 5:48 UT (hono, 4,963 km from the epicenter). The halei gauge recorded an amplitude of 1.38 m above normal sea level at the first tsunami strike. The tsunami reached the island of Molokai (kaun, 5,044 km from the earthquake's epicenter) at 5:55 UT. The tsunami's arrival on the island of Hawaii was recorded at 6:12 UT (milo, 5,284 km from the earthquake's epicenter) and at 6:13 UT (hilo, 5,285 km from the epicenter). Overall, the tsunami's arrival was observed in the Hawaiian Islands from 3:37 to 6:13 UT, with initial amplitudes ranging from 21 to 139 cm. Estimating the average speed (Table 1), the tsunami propagated at an average speed of 215 m/s.

Table 1. Parameters of tsunami propagation according to the data of tsunami monitoring stations

Tsunami monitoring station	Distance between tsunami monitoring station and earthquake's epicenter, km	Time of the tsunami's arrival, UT	Average speed of tsunami propagation, km/s	Maximum amplitude of wave height, m
midx	3272	July 30, 2025 3:37	215.5	1
fren	4252	July 30, 2025 4:52	216.1	0.21
hanl	4793	July 30, 2025 5:35	215.3	0.91
john	4773	July 30, 2025 5:33	215.6	0.43
halei	4932	July 30, 2025 5:46	215.2	1.39
hono	4963	July 30, 2025 5:48	215.4	0.41
kaun	5044	July 30, 2025 5:55	215.0	0.37
milo	5284	July 30, 2025 6:12	215.8	0.23
hilo	5285	July 30, 2025 6:13	215.4	1.29

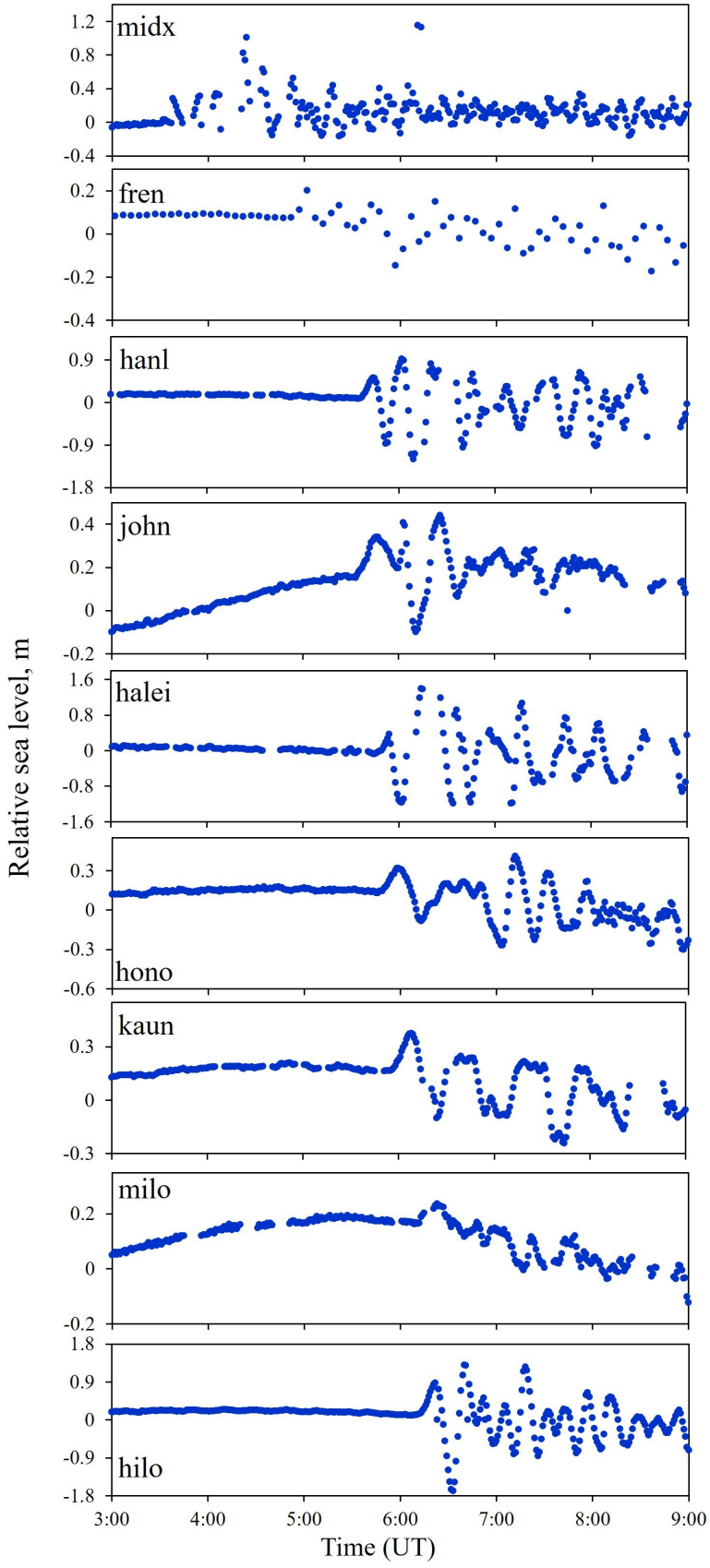

Figure 4. Variations in relative sea level according to data from sensors located on the Hawaiian Islands (Figure 2).

5. Remote Ionospheric Effect of a Tsunami

Of the 32 GPS satellites, six were within the hn1c receiver's coverage area during the time interval from 3:00 to 7:30 UT. Figure 5, along with the hn1c receiver's location, shows the satellite path projections onto the ionosphere for the six selected GPS satellites whose data were used in the analysis. The flight times are indicated on the paths.

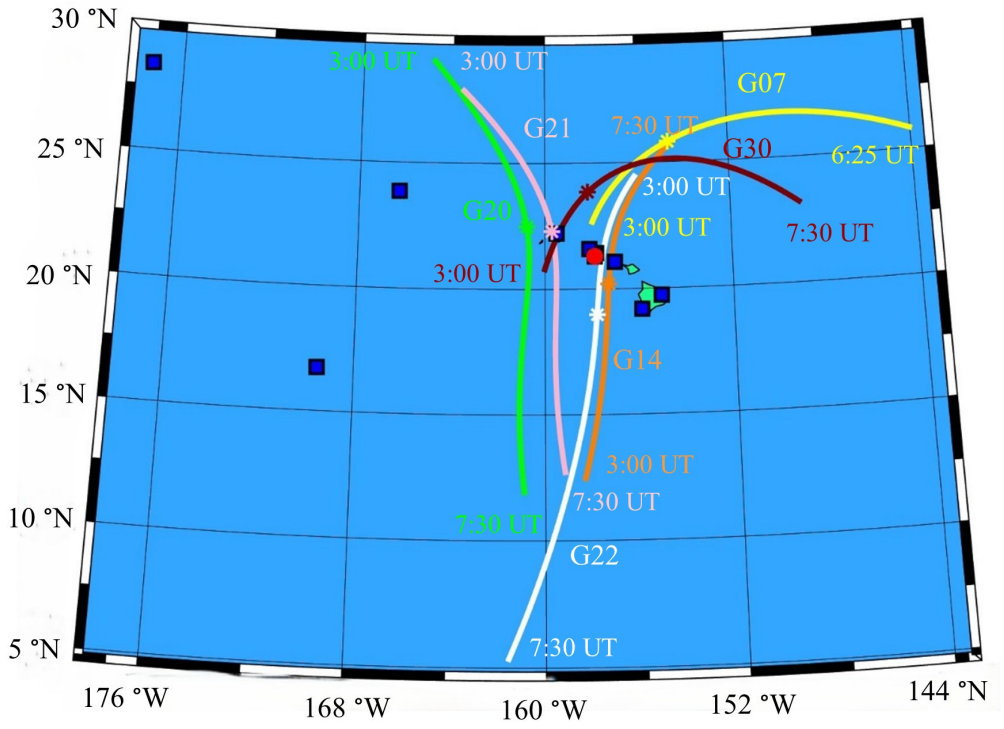

Figure 5. Geographic map with GPS satellite path projections for the hn1c receiving station for July 30, 2025. Time is indicated at the beginning and end of the path projection. The hn1c receiving station is indicated by a red circle. Locations of tsunami monitoring stations in the Hawaiian Islands are indicated by blue squares (Figure 2). Symbol (*) with corresponding color indicates GPS position at the onset of increased TEC variations.

Figure 6 presents 30-second data on the TEC variations after applying 7th-order Butterworth bandpass filtering. As can be seen from Figure 6, the temporal variations in the TEC exhibit variations of increased intensity. In particular, according to data from the G07 satellite, increased variations in the TEC were observed from 4:43 UT with an amplitude of up to 0.6 TECU. At the time when increased variations began, the satellite was located 4,775 km from the earthquake's epicenter off the coast of the Kamchatka Peninsula. According to data from the G14 satellite, such variations were observed from 4:56 UT (5,094 km from the earthquake's epicenter) with an amplitude of up to 0.58 TECU. Similarly, for the time of the onset of variations and their amplitude, based on observations on other satellites, the following was obtained: G20 satellite – 4:39 UT (4,691 km from the earthquake epicenter) with an amplitude of up to 0.63 TECU, G21 satellite – 4:43 UT (4,773 km from the earthquake epicenter) with an amplitude of up to 0.6 TECU, G22 satellite – 5:00 UT (5,188 km from the earthquake epicenter) with an amplitude of up to 0.57 TECU, G30 satellite – 4:41 UT (4,727 km from the earthquake epicenter) with an amplitude of up to 0.61 TECU.

As can be seen from Table 2, all satellites, and particularly those whose trajectory projections were close to the receiver (e.g., G07, G22, G30), demonstrate a clear lead time (48–66 minutes) for the onset of increased TEC variations compared to the first tsunami arrival at the same distance from the earthquake epicenter. Table 2 shows a slight decrease in the amplitude of variations as the distance from the earthquake epicenter increases.

Table 2. Parameters of increased TEC variations at hn1c receiving station

GPS satellite	Distance of onset of increased TEC variations from the earthquake's epicenter, km	Time of onset of increased TEC variations (UT)	Estimated arrival time of the tsunami at the distance of onset of increased TEC variations (UT)	Maximum amplitude of increased TEC variations, TECU
G07	4775	4:43 30.07.2025	5:34 30.07.2025	0.6
G14	5108	4:56 30.07.2025	5:58 30.07.2025	0.58
G20	4691	4:39 30.07.2025	5:27 30.07.2025	0.63
G21	4773	4:43 30.07.2025	5:34 30.07.2025	0.6
G22	5188	5:00 30.07.2025	6:06 30.07.2025	0.57
G30	4727	4:41 30.07.2025	5:30 30.07.2025	0.61

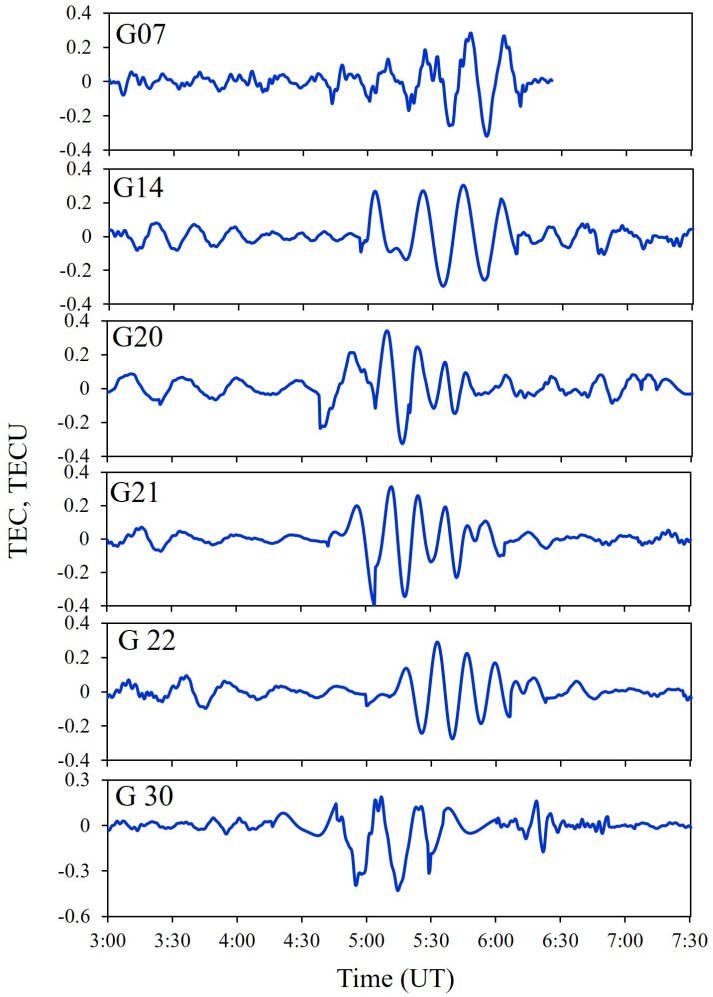

Figure 6. Filtered variations of the TEC recorded at the hn1c receiving station, satellite numbers are indicated in the figure field.

To perform a frequency analysis of the TEC variations in this study, a spectral analysis based on a wavelet transform was performed. As can be seen from Figure 7, the areas of increased amplitude of the TEC variations are far from the boundaries of the "cone of influence." The data in Figure 7 indicate that ionospheric density variations are observed from 4:39 UT (G20), from 4:41 UT (G30), from 4:43 UT (G21), from 4:56 UT (G14) and from 5:00 UT (G22). As can be seen from Figure 5, the satellite G07 left the hn1c station's coverage area at 6:25 UT. Therefore, for G07 a scalogram was constructed for the time interval from 3:00 to 6:25 UT.

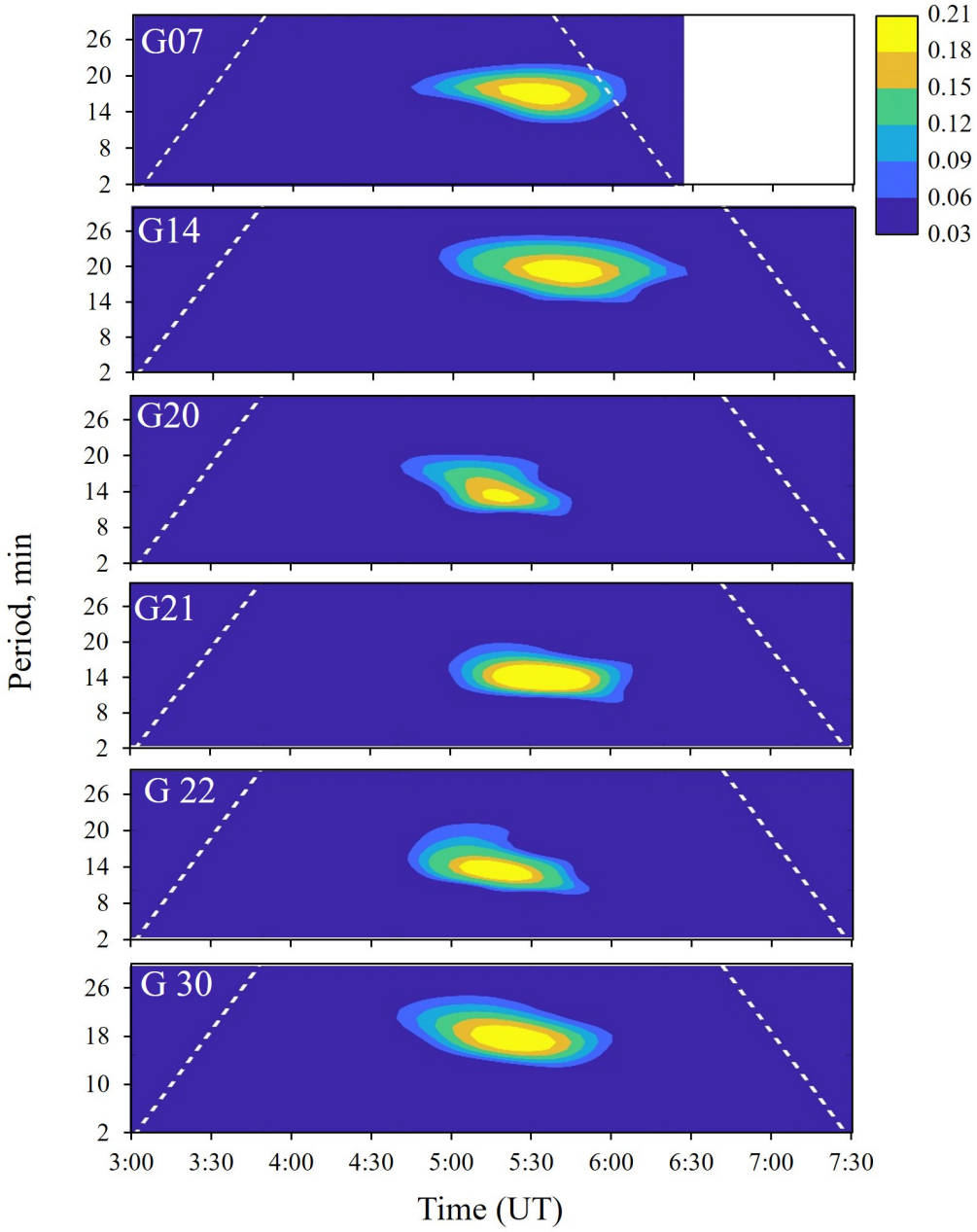

Figure 7. Scalograms of filtered variations of the TEC recorded at the hn1c receiving station, satellite numbers are indicated in the figure field, the white lines are the cone of influence.

Table 3 shows that the range of periods of TEC variations from 9 to 25 minutes corresponds to the range of atmospheric internal gravity waves. Significant changes in the spectral composition depending on the position of the satellite relative to the epicenter at the moment of the beginning of observation of increased TEC variations are not observed. As can be seen from Figure 7, low-frequency disturbances are registered earlier than high-frequency ones.

Analysis of signal scalograms for all six GPS satellites considered in the present paper reveals well-organized wave trains of traveling ionospheric disturbances (TIDs) that were detected over the islands in the far zone from the epicenter of the Kamchatka earthquake on the same day. These waves are associated with the propagation of IGWs.

Table 3. Spectral characteristics of increased TEC variations at hn1c receiving station

GPS satellite	Distance of onset of increased TEC variations from the earthquake's epicenter, km	Time of onset of increased TEC variations, UT	Period of increased TEC variations, min
G07	4775	4:43 30.07.2025	12–22.5
G14	5094	4:56 30.07.2025	14–25
G20	4691	4:39 30.07.2025	10–20
G21	4773	4:43 30.07.2025	9–21
G22	5188	5:00 30.07.2025	9–20
G30	4727	4:41 30.07.2025	13–25

6. Discussion

As demonstrated in the present paper, using data from a GPS receiver located in the Hawaiian Islands, well-organized wave trains of traveling ionospheric disturbances (TIDs) were detected over the islands in the far zone from the epicenter of the Kamchatka earthquake on the same day. Periods of these waves correspond to the propagation of IGWs.

It should be noted that the hypothesis that TIDs are propagating atmospheric IGWs (entering the ionosphere due to the presence of vertical velocity) was put forward quite a long time ago (see, for example, [*Hines*, 1960]). Since then, it has found experimental confirmation, the most recent of which is associated with the recording of TIDs from TEC variations using GPS [*Afraimovich and Perevalova*, 2006].

Under quiet geomagnetic conditions, these TIDs can be caused by a tsunami, which, as is known [*Golitsyn and Klyatskin*, 1967], generates IGWs during its propagation. Moreover, the appearance of TIDs over the Hawaiian Islands significantly precedes the arrival of the tsunami. Thus, while the first tsunami detection at monitoring stations near the vicinity of GPS receiver was recorded at 3:37 UT, TIDs were detected by all satellites examined between 4:39 and 5:00 UT, i.e., the IGW precedes the tsunami by at least several tens of minutes.

Analysis of signal scalograms for all six GPS satellites, considered in the present paper, well-organized wave trains of traveling ionospheric disturbances (TIDs) were detected over the islands in the far zone from the epicenter of the Kamchatka earthquake on the same day. These waves are associated with the propagation of IGWs.

The conclusion that atmospheric waves driven by sea wave move faster the latter is easy to understand if we consider the dispersion relation for atmospheric internal gravity waves [*Gossard and Hooke*, 1975]:

$$\omega^2 = \frac{4H^2k_x^2\omega_g^2}{1+4H^2k^2},$$

where $k^2 = k_x^2 + k_z^2$ is the wave vector, ω_g is the Brunt–Väisälä frequency, and H is the characteristic scale of the atmosphere. From the dispersion relation it is easy to see that the frequency of atmospheric internal waves ω can vary from close to zero (when the wave vector is close to vertical) to ω_g (when the wave vector is almost horizontal). For IGWs, the group velocity is perpendicular to the phase velocity, so that the wave energy propagates at a right angle to the direction of propagation of the wave front. Low-frequency waves (when the frequency is close to zero and the wave vector is almost vertical) have the fastest group velocity, and this velocity is directed almost horizontally. In other words, weakly oscillating horizontal structures are very efficient in distributing energy horizontally.

In addition, the group velocity of atmospheric waves is greater than or equal to their horizontal phase velocity. In turn, the horizontal phase velocity of an atmospheric wave (according to its radiation condition) is greater than the horizontal propagation velocity of the tsunami.

This is why a specific shape of the ionospheric signal is observed: low-frequency signals are recorded first, followed by high-frequency signals. In other words, this shape of the signal indicates that the tsunami is preceded by an atmospheric IGW.

7. Conclusion

Thus, the tsunami generated after the Kamchatka earthquake and atmospheric internal gravity waves (IGWs) driven by the tsunami according to the radiation condition can propagate at considerable distance from the epicenter. At large distances from the epicenter, the IGWs emitted by the tsunami and having faster group velocity must be ahead of the sea wave. Since the IGWs have a vertical component of the velocity they can reach the ionosphere and cause ionospheric density variations. In the ionosphere this advance of IGWs becomes so noticeable that it can be reliably recorded with modern instruments. In this study, the phenomenon of IGWs driven by tsunami and finally propagating faster than a sea wave (tsunami) was experimentally verified using a tidal tsunami monitoring station and GPS measurements of the TEC variations in the upper ionosphere. A specific spectral shape of ionospheric signal caused by the IGWs has been demonstrated, which indicates the earlier arrival of the ionospheric signal compared to the arrival of the tsunami. The effect of IGWs propagating faster than the tsunami that drives them and specific spectral shape of ionospheric signal caused by the IGWs can be used as an additional instrument for tsunami early warning systems.

Acknowledgments. This research was carried out as part of the State Task of Schmidt Institute of Physics of the Earth of Russian Academy of Sciences and as part of the State Task of the Sadovsky Institute of Geosphere Dynamics of Russian Academy of Sciences (topic no. 125012700798-8 “Transformation of Geophysical Fields as the Main Factor in Intergeospheric Interactions”).

References

Afraimovich E. L. and Perevalova N. P. GPS-monitoring of the Earth’s upper atmosphere. — Irkutsk : SI SC RRS ESSC SB RAMS, 2006. — 480 p. — (In Russian).

Argus D. F., Gordon R. G. and DeMets C. Geologically current motion of 56 plates relative to the no-net-rotation reference frame // Geochemistry, Geophysics, Geosystems. — 2011. — Vol. 12, no. 11. — https://doi.org/10.1029/2011gc003751

Azeem I., Vadas S. L., Crowley G., et al. Traveling ionospheric disturbances over the United States induced by gravity waves from the 2011 Tohoku tsunami and comparison with gravity wave dissipative theory // Journal of Geophysical Research: Space Physics. — 2017. — Vol. 122, no. 3. — P. 3430–3447. — https://doi.org/10.1002/2016ja023659

Bürgmann R., Kogan M. G., Steblov G. M., et al. Interseismic coupling and asperity distribution along the Kamchatka subduction zone // Journal of Geophysical Research: Solid Earth. — 2005. — Vol. 110, B7. — https://doi.org/10.1029/2005JB003648

Butterworth S. On the theory of filter amplifiers // Experimental Wireless and the Wireless Engineer. — 1930. — Vol. 7. — P. 536–541.

Chandrasekhar E., Prabhudesai S. S., Seemala G. K., et al. Multifractal detrended fluctuation analysis of ionospheric total electron content data during solar minimum and maximum // Journal of Atmospheric and Solar-Terrestrial Physics. — 2016. — Vol. 149. — P. 31–39. — https://doi.org/10.1016/j.jastp.2016.09.007

Fedotov S. A. On the seismic cycle, the possibility of quantitative seismic zoning, and long-term seismic forecasting // Seismic zoning of the USSR. — Moscow : Nauka, 1968. — P. 121–150. — (In Russian).

Golitsyn G. S. and Klyatskin V. I. Atmosphere oscillations caused by Earth’s surface displacement // Izvestiya of the Academy of Sciences of the USSR. Atmospheric and Oceanic Physics. — 1967. — Vol. 3, no. 10. — P. 1044–1052. — (In Russian).

Gossard E. E. and Hooke W. H. Waves in the Atmosphere: Atmospheric Infrasound and Gravity Waves-Their Generation and Propagation. — Amsterdam, Oxford, New York : Elsevier Scientific Publishing Company, 1975. — 456 p.

Heidarzadeh M. and Satake K. Waveform and Spectral Analyses of the 2011 Japan Tsunami Records on Tide Gauge and DART Stations Across the Pacific Ocean // Pure and Applied Geophysics. — 2013. — Vol. 170, no. 6–8. — P. 1275–1293. — https://doi.org/10.1007/s00024-012-0558-5

Hines C. O. Internal atmospheric gravity waves at ionospheric heights // Canadian Journal of Physics. — 1960. — Vol. 38, no. 11. — P. 1441–1481. — https://doi.org/10.1139/p60-150

Hubbard J. and Bradley K. M7.4 earthquake strikes the Kamchatka Peninsula: Questions about megaquake advisories, revived? // Earthquake Insights. — 2025. — https://doi.org/10.62481/a8be96de

Inchin P. A., Heale C. J., Snively J. B., et al. Numerical modeling of tsunami-generated acoustic-gravity waves in mesopause airglow // Journal of Geophysical Research: Space Physics. — 2022. — Vol. 127, no. 8. — https://doi.org/10.1029/2022ja030301

Jayachandran P. T., Hosokawa K., Shiokawa K., et al. GPS total electron content variations associated with poleward moving Sun-aligned arcs // Journal of Geophysical Research: Space Physics. — 2012. — Vol. 117, A5. — https://doi.org/10.1029/2011JA017423

Kotenko T., Zaytsev A. and Pelinovsky E. Short report: data from the post tsunami field survey after the tsunami (29.07.2025) in Severo-Kurilsk (Paramushir Island, Northern Kuriles), via Tsunami Bulletin Board. Received 04 August 2025. — 2025a. — URL: https://www.ngdc.noaa.gov/hazel/view/hazards/tsunami/runup-more-info/39518 (visited on 11/01/2025).

Kotenko T., Zaytsev A. and Pelinovsky E. Tsunami Inundation Report at Baikovo in Shumshu Island, sent via Tsunami Bulletin Board. 05 August 2025. — 2025b. — URL: https://www.ngdc.noaa.gov/hazel/view/hazards/tsunami/runup-more-info/39544 (visited on 11/01/2025).

Koulakov I. Y., Dobretsov N. L., Bushenkova N. A., et al. Slab shape in subduction zones beneath the Kurile-Kamchatka and Aleutian arcs based on regional tomography results // Russian Geology and Geophysics. — 2011. — Vol. 52, no. 6. — P. 650–667. — https://doi.org/10.1016/j.rgg.2011.05.008

Lobkovsky L. I., Vladimirova I. S., Alekseev D. A., et al. Two-Element Keyboard Model of Generation of the Strongest Subduction Earthquakes // Doklady Earth Sciences. — 2021. — Vol. 496, no. 1. — P. 72–75. — https://doi.org/10.1134/s1028334x2101013x

Meyer Y. Wavelets: Algorithms and applications. — Philadelphia : Society for Industrial, Applied Mathematics, 1993. — 133 p.

NOAA / PMEL / Center for Tsunami Research. Kamchatka Tsunami, July 29, 2025. — 2025. — URL: https://nctr.pmel.noaa.gov/kamchatka20250729/ (visited on 11/01/2025).

Prytkov A. S., Vasilenko N. F. and Frolov D. I. Recent geodynamics of the Kuril subduction zone // Russian Journal of Pacific Geology. — 2017. — Vol. 11, no. 1. — P. 19–24. — https://doi.org/10.1134/s1819714017010067

PTWC. 29 July 2025, Mw 8.8, Kamchatka Peninsula, Russia Tsunami. Sea Level Observations (IOC, PNG 253 KB). — 2025. — URL: https://www.weather.gov/itic-car/29july2025_kamtchatka_tsunami (visited on 11/01/2025).

Riabova S. Application of wavelet analysis to the analysis of geomagnetic field variations // Journal of Physics: Conference Series. — 2018. — Vol. 1141. — P. 012146. — https://doi.org/10.1088/1742-6596/1141/1/012146

Riabova S. A. Study of the Multifractality of Geomagnetic Variations at the Belsk Observatory // Doklady Earth Sciences. — 2022. — Vol. 507, S2. — S299–S303. — https://doi.org/10.1134/s1028334x22700489

Riabova S. A. and Shalimov S. L. Ionospheric Response of Earthquakes in the Philippines from November to December 2023 // Izvestiya, Physics of the Solid Earth. — 2024a. — Vol. 60, no. 6. — P. 1016–1025. — https://doi.org/10.1134/s1069351324701015

Riabova S. A. and Shalimov S. L. On the Geomagnetic and Ionospheric Variations after the 2023 Strong Eruption of the Shiveluch Volcano // Izvestiya, Physics of the Solid Earth. — 2024b. — Vol. 60, no. 4. — P. 612–621. — https://doi.org/10.1134/s1069351324040013

Riabova S. A. and Shalimov S. L. Response of the Lower and Upper Ionosphere after the Eruption of Shiveluch Volcano on April 10, 2023 // Geomagnetism and Aeronomy. — 2024c. — Vol. 64, no. 1. — P. 94–101. — https://doi.org/10.1134/s001679322360087x

Rozhnoi A., Shalimov S., Solovieva M., et al. Tsunami-induced phase and amplitude perturbations of subionospheric VLF signals // Journal of Geophysical Research: Space Physics. — 2012. — Vol. 117, A9. — https://doi.org/10.1029/2012ja017761

Shalimov S. L., Nesterov I. A. and Vorontsov A. M. On the GPS-based ionospheric perturbation after the Tohoku earthquake of March 11, 2011 // Izvestiya, Physics of the Solid Earth. — 2017. — Vol. 53, no. 2. — P. 262–273. — https://doi.org/10.1134/S1069351317020112

Soloviev S. L. Methods of tsunami prediction // Vestnik AN SSSR. — 1972. — No. 5. — P. 72–81. — (In Russian).

Torrence C. and Compo G. P. A Practical Guide to Wavelet Analysis // Bulletin of the American Meteorological Society. — 1998. — Vol. 79, no. 1. — P. 61–78. — https://doi.org/10.1175/1520-0477(1998)079<0061:apgtwa>2.0.co;2

USGS. M 9.0 – 89 km ESE of Petropavlovsk-Kamchatsky, Russia. — 2010. — URL: https://earthquake.usgs.gov/earthquakes/eventpage/official19521104165830_30/executive (visited on 11/01/2025).

USGS. M 8.8 – 2025 Kamchatka Peninsula, Russia Earthquake. — 2025. — URL: https://earthquake.usgs.gov/earthquakes/eventpage/pt25210002/executive (visited on 11/01/2025).

Wen Y. and Jin S. Traveling Ionospheric Disturbances Characteristics during the 2018 Typhoon Maria from GPS Observations // Remote Sensing. — 2020. — Vol. 12, no. 4. — P. 746. — https://doi.org/10.3390/rs12040746

Wirth E. A., Sahakian V. J., Wallace L. M., et al. The occurrence and hazards of great subduction zone earthquakes // Nature Reviews Earth & Environment. — 2022. — Vol. 3, no. 2. — P. 125–140. — https://doi.org/10.1038/s43017-021-00245-w